Molecular Therapy
Original Article

Tumor Antigen and Receptor Densities Regulate Efficacy of a Chimeric Antigen Receptor Targeting Anaplastic Lymphoma Kinase

Alec J. Walker,[1,4] Robbie G. Majzner,[2,4] Ling Zhang,[1] Kelsey Wanhainen,[1] Adrienne H. Long,[1] Sang M. Nguyen,[1] Paola Lopomo,[1] Marc Vigny,[3] Terry J. Fry,[1] Rimas J. Orentas,[1] and Crystal L. Mackall[2]

[1]Pediatric Oncology Branch, Center for Cancer Research (CCR), National Cancer Institute (NCI), NIH, Bethesda, MD 20892, USA; [2]Department of Pediatrics, Stanford University School of Medicine, Stanford, CA 94305, USA; [3]INSERM/UPMC, Institut du Fer à Moulin, 75005 Paris, France

We explored the utility of targeting anaplastic lymphoma kinase (ALK), a cell surface receptor overexpressed on pediatric solid tumors, using chimeric antigen receptor (CAR)-based immunotherapy. T cells expressing a CAR incorporating the single-chain variable fragment sequence of the ALK48 mAb linked to a 4-1BB-CD3ζ signaling domain lysed ALK-expressing tumor lines and produced interferon-gamma upon antigen stimulation but had limited anti-tumor efficacy in two xenograft models of human neuroblastoma. Further exploration demonstrated that cytokine production was highly dependent upon ALK target density and that target density of ALK on neuroblastoma cell lines was insufficient for maximal activation of CAR T cells. In addition, ALK CAR T cells demonstrated rapid and complete antigen-induced loss of receptor from the T cell surface via internalization. Using a model that simultaneously modulated antigen density and CAR expression, we demonstrated that CAR functionality is regulated by target antigen and CAR density and that low expression of either contributes to limited anti-tumor efficacy of the ALK CAR. These data suggest that stoichiometric relationships between CAR receptors and target antigens may significantly impact the anti-tumor efficacy of CAR T cells and that manipulation of these parameters could allow precise tuning of CAR T cell activity.

INTRODUCTION

Anaplastic lymphoma kinase (ALK) is a transmembrane receptor tyrosine kinase with important roles in mesodermal differentiation in *Drosophila*, eye development in *C. elegans*, neural crest-derived iridiphore development in zebrafish, and the developing nervous system in mammals.[1] However, ALK is largely absent from nonmalignant post-natal tissues. Cancer-associated ALK was first described as a truncated oncogenic intracellular fusion protein partnered with nucleophosmin (NPM) in anaplastic large cell leukemia (ALCL)[2] and is fused to echinoderm microtubule-associated protein-like 4 (EML4) in ~9% of non-small-cell lung carcinomas (NSCLCs).[3,4] Activating mutations of full-length ALK are present in 8%–12% of neuroblastomas[5,6] and are responsible for a sizable fraction of familial neuroblastoma.[5] Overexpression of mutated or wild-type ALK can drive oncogenesis in vitro and in vivo[6–9] and correlates with poor prognosis in patients with neuroblastoma.[10,11] Strategies to target ALK in neuroblastoma using small molecule inhibitors have seen limited success, potentially due to resistant kinase mutations.[12] Targeting ALK overexpression, independently of the highly mutated kinase domain, could provide clinical benefit without risk for this type of mutagenic escape.

T cells engineered to express chimeric antigen receptors (CARs) have recently joined the rapidly growing repertoire of immunotherapeutics available to treat cancer. CARs link the epitope specificity of a monoclonal antibody to the cytolytic capacity of an activated T cell, allowing targeting of tumors expressing cognate, cell surface antigen in a major histocompatibility complex (MHC)-independent manner. CAR T cells have demonstrated significant activity against B cell malignancies,[13–19] but the results in solid tumors have not yet been as clinically significant.[20–22] Antibodies have been developed against the extracellular domain of ALK[23] and can mediate lytic activity against neuroblastoma cell lines in culture,[24] raising the possibility that ALK may be a viable CAR T cell target. Here we report a CAR T cell therapy targeting cell surface ALK, and we demonstrate that antigen density and CAR density coordinately regulate ALK CAR T cell effector functions. Additionally, we identify antigen-dependent CAR down-modulation as a factor limiting CAR T cell anti-tumor activity, suggesting that manipulation of CAR surface expression and recycling could enhance CAR T cell efficacy.

RESULTS

Overexpression of ALK in Pediatric Solid Tumors

To evaluate ALK as a potential target for T cell immunotherapy, we assessed *ALK* RNA expression across an array of pediatric tumor cell lines, patient-derived xenografts, and tumor biopsies accessed through the Pediatric Tumor Affymetrix Database[25] (NCI Pediatric

Received 21 December 2016; accepted 9 June 2017;
http://dx.doi.org/10.1016/j.ymthe.2017.06.008.

[4]These authors contributed equally to this work.

Correspondence: Crystal L. Mackall, Department of Pediatrics, Stanford University of Medicine, 265 Campus Way St G3141A, Stanford, CA 94305, USA.
E-mail: cmackall@stanford.edu

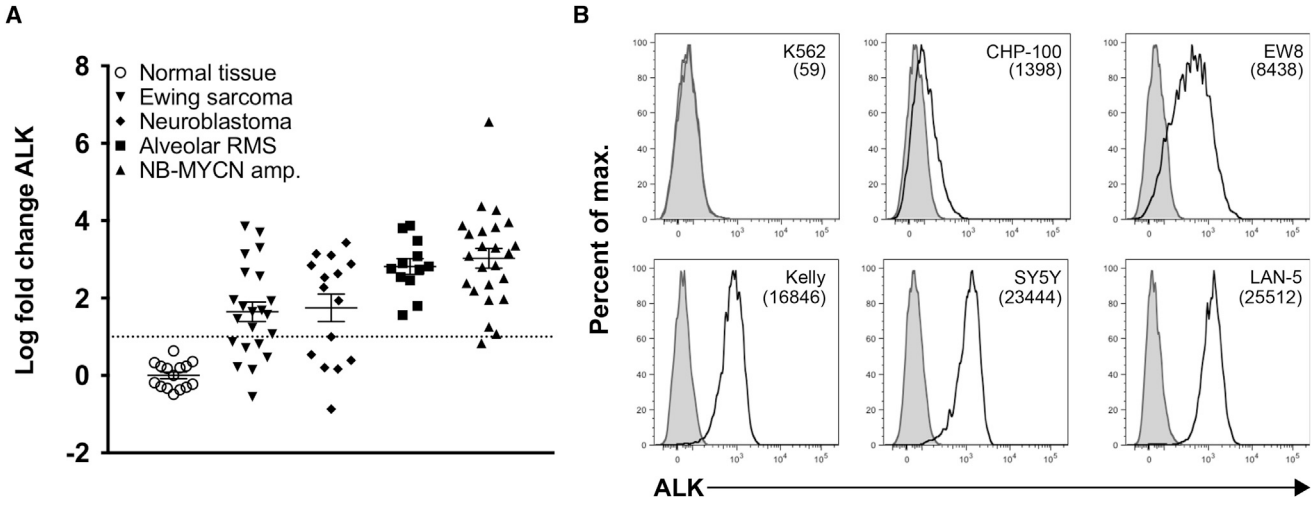

Figure 1. Expression of Anaplastic Lymphoma Kinase in Pediatric Solid Tumors

Affymetrix mRNA expression data were obtained from the NIH Pediatric Oncology Branch Oncogenomics Database. (A) ALK expression is shown for a normal tissue array (n = 15) and a collection of Ewing sarcoma (EWS, n = 22), alveolar rhabdomyosarcoma (ARMS, n = 12), neuroblastoma (NB, n = 15), and MYCN-amplified neuroblastoma (NB-MYCN amp., n = 24) samples. Error bars represent the mean ± SEM. (B) Expression of cell surface ALK protein was evaluated and quantified by flow cytometry. Representative histograms and quantifications representing the mean number of ALK molecules per cell are shown for human neuroblastoma (CHP-100, SY5Y, Kelly, and LAN-5) and Ewing sarcoma (EW8) cell lines. The human chronic myelogenous leukemia line, K562, was used as an ALK-negative control. ALK expression on cell lines is representative of five experiments.

Oncology Branch). *ALK* mRNA was overexpressed in neuroblastomas, Ewing sarcomas, and alveolar rhabdomyosarcomas compared to normal tissue (Figure 1A). Using a previously described mouse monoclonal antibody, ALK48, directed against the extracellular domain of ALK,[23] we observed surface expression of ALK in human-derived neuroblastoma and Ewing sarcoma cell lines by flow cytometry, at levels ranging from 1,400 to 25,000 molecules per cell (Figure 1B). We thus predicted that ALK would provide a viable target for CAR-mediated immunotherapy.

Development of CARs Targeting ALK

To evaluate the potential for ALK CAR T cell therapy directed against neuroblastoma, we built and characterized several CARs incorporating single chain variable fragments (scFvs) targeting ALK and either CD28-CD3ζ or CD8α-4-1BB-CD3ζ signaling motifs. After retroviral transduction into human T cells, CARs built from two scFvs (ALK53 and ALK58)[23] showed either negligible expression or modest activity in vitro (data not shown). However, CARs built from the ALK48 scFv (ALK48.CD28.ζ and ALK48.4-1BB.ζ) expressed on the T cell surface (Figures S1A and S1B), produced interferon-gamma (IFN-γ) upon antigen stimulation, and specifically lysed an ALK-expressing tumor cell line in vitro (Figures S1C and S1D). Previous studies have demonstrated that the addition of a spacer between the CAR transmembrane domain and scFv can significantly impact CAR T cell activity.[26,27] We constructed two additional long ALK48 CARs bearing the CH2-CH3 domain of human IgG1 (ALK48L.CD28.ζ and ALK48L.4-1BB.ζ). These long CARs expressed at similar levels to short CARs on the T cell surface, but long ALK48 CAR T cells showed considerably diminished cytokine production and cytolytic activity. Based on these data and emerging evidence that CARs bearing the 4-1BB-CD3ζ motif are less prone to exhaustion in vivo,[28] we selected the ALK48.4-1BB.ζ CAR (hereafter referred to as the ALK CAR) (Figure 2A) for further investigation.

We consistently noted that the ALK CAR expressed moderately on the T cell surface (Figure 2B), contrary to several other high-expressing CARs we have worked with targeting CD19 and CD22.[29] ALK CAR T cells produced IFN-γ when exposed to the ALK-expressing neuroblastoma cell lines SY5Y and Kelly (Figure 2C). Additionally, in vivo function of the ALK CAR against SY5Y and Kelly xenografts was evaluated. Tumor growth in mice treated with ALK CAR was significantly attenuated compared to mock-treated mice in both models (Figure 2D). However, most mice in the CAR T cell-treated groups eventually succumbed to tumor, suggesting a need to better understand factors limiting the efficacy of the ALK CAR.

Optimal In Vitro and In Vivo ALK CAR T Cell Function Requires High Tumor Antigen Expression

While solid tumors mediate suppression within the tumor microenvironment (TME), we have previously reported that neuroblastomas mediate diminished local immunosuppression when compared to sarcomas.[30] These data raise the prospect that factors other than a locally immunosuppressive TME could contribute to tumor escape in this model system. To assess the impact of ALK expression on ALK CAR T cell efficacy, we expressed the transmembrane and extracellular domains of ALK at varying levels in the NALM-6-GFP-luciferase leukemia line (NALM-6-GL). We have previously shown that NALM-6-GL can be efficiently cleared by CAR T cells targeting CD19 and CD22,[29] and, thus, it is a suitable model for the evaluation of CAR T cell efficacy in vitro and in vivo.

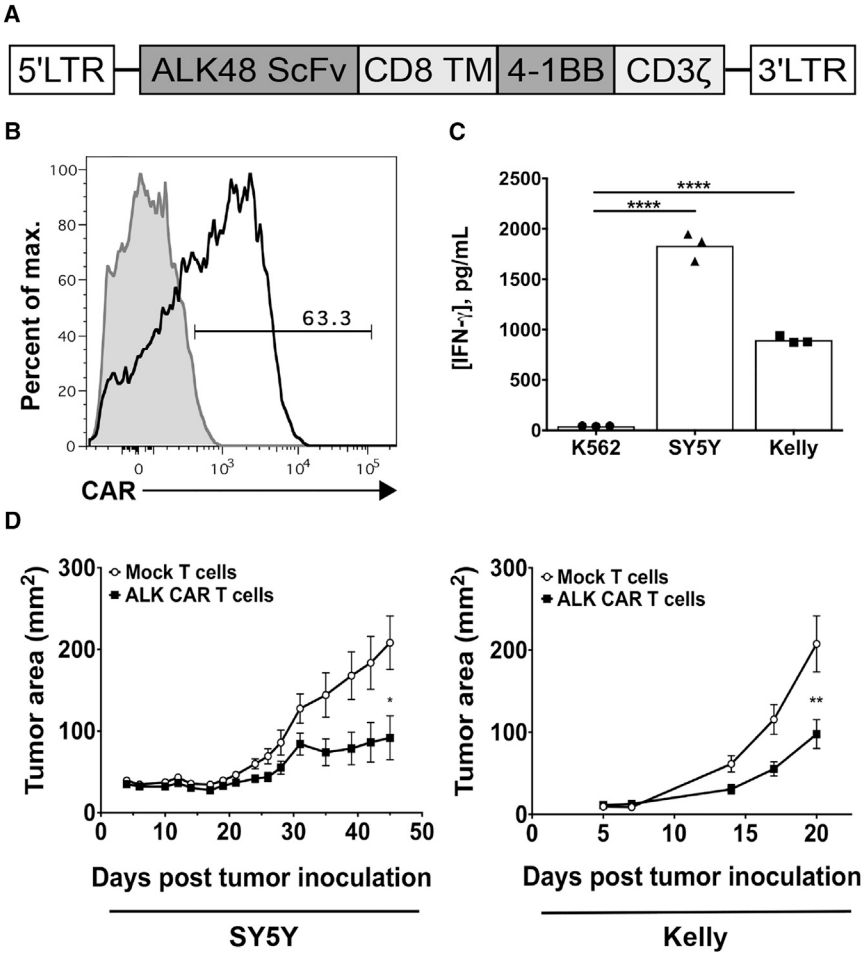

Figure 2. Design and Characterization of a Chimeric Antigen Receptor Targeting ALK

(A) The ALK48 single-chain variable fragment was cloned into an MSGV1 retroviral expression vector containing a CD8α transmembrane-4-1BB-CD3ζ signaling motif to create the MSGV.ALK48.4-1BB.ζ construct encoding the ALK CAR. (B) Human peripheral blood mononuclear cells (PBMCs) were transduced with MSGV.ALK48.4-1BB.ζ CAR retroviral supernatant, and surface ALK CAR expression was evaluated by flow cytometry. (C) ALK CAR T cells were assayed for IFN-γ release after co-incubation with tumor targets. Differences in ALK CAR production of IFN-γ were evaluated by a one-way ANOVA followed by a Tukey's multiple comparisons test, and they are representative of three experiments with different PBMC donors. (D) In vivo efficacy of ALK CAR T cells was assessed in two xenograft models of neuroblastoma. Growth curves of SY5Y or Kelly tumors after treatment with ALK CAR or mock-transduced T cells are shown. Differences in tumor growth were determined using a repeated-measures ANOVA. Error bars represent SEM (n = 5 mice per group [SY5Y] and n = 10 mice per group [Kelly]). In vivo experiments were repeated twice for each tumor model with different PBMC donors.

Surface ALK expression varied up to 75-fold across the library of lines (Figure 3A), and maximum ALK expression was ~15 times higher than maximum ALK expression observed in neuroblastoma cell lines. Notably, ALK CAR T cells lysed ALK^{high} NALM-6-GL-ALK cells (~450,000 copies of ALK) more effectively than ALK^{low} cells (~18,000 copies of ALK) (Figure 3B). ALK CAR T cells were then co-incubated with NALM-6-GL-ALK cell lines comprising a broad range of ALK densities. Production of IFN-γ, interleukin-2 (IL-2), and tumor necrosis factor (TNF)-α showed a sharp threshold dependent on tumor antigen expression, and half-maximum cytokine production was reached at significantly lower antigen densities for IFN-γ compared to IL-2 (Figures 3C and 3D). Consistent with in vitro results, ALK CAR T cells significantly prevented outgrowth of ALK^{high}, but not ALK^{low}, leukemia in vivo (Figure 3E). As neuroblastoma ALK levels were comparable to those found on ALK^{low} NALM-6, these data suggest that the ALK levels expressed on neuroblastomas tested are not sufficient to induce maximal CAR functionality, and they provide evidence that CAR signal strength and effector function are limited by tumor antigen density in this model system.

CAR T Cells Show Antigen-Dependent Receptor Down-Modulation

During in vivo experiments with the ALK CAR, we noted that we could not detect ALK CAR-positive T cells in the blood of tumor-bearing mice. This phenomenon could result from poor persistence of transduced CAR T cells or, alternatively, from loss of CAR receptor in transduced T cells in vivo. To explore these possibilities, we inoculated mice with ALK^{high} NALM-6-GL tumor and subsequently adoptively transferred ALK CAR T cells. Indeed, ALK CAR surface expression could not be detected at 5 or 12 days after transfer into mice (Figure 4A, top panel). However, ALK CAR^{+} T cells could be readily detected by qPCR from peripheral blood of these mice (Figure 4A, bottom panel), suggesting that T cells transduced with the ALK CAR persist in vivo but lose surface expression of the CAR.

To determine whether this apparent loss of CAR from the cell surface was in part antigen dependent, we co-incubated ALK CAR T cells with ALK^{high} or ALK^{-} NALM6-GL tumors in vitro, and we evaluated CAR expression by flow cytometry. ALK CARs were profoundly down-modulated from the cell surface after antigen encounter (Figure 4B). This down-modulation was abrogated in cells maintained at 4°C, consistent with receptor internalization rather than CAR blockade by shed antigen (Figure S2A). Receptor surface expression was similarly diminished in CD19 CAR T cells co-incubated with CD19^{+} NALM6-GL tumors compared to CD19 CAR T cells co-incubated with CD19^{KO} NALM6-GL (Figure 4B), suggesting that this is a conserved phenomenon in CAR T cells. Using T cells expressing a

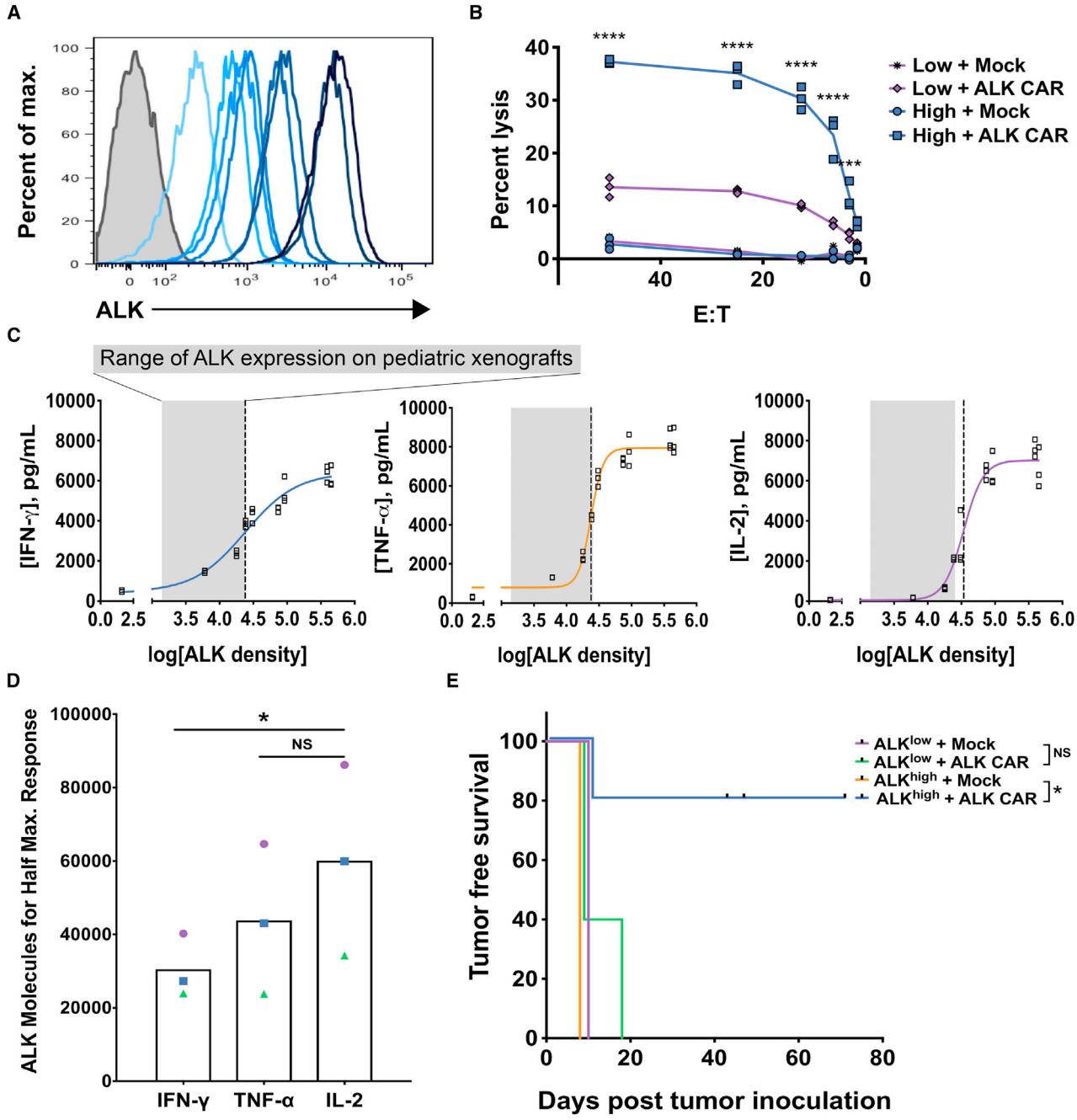

Figure 3. In Vitro and In Vivo Functionality of ALK CAR across a Range of Tumor Antigen Densities

(A) The human B cell leukemia line, NALM-6, expressing GFP-luciferase (NALM-6-GL) was lentivirally transduced to create clones expressing a range of cell surface ALK expression. (B) NALM-6-GL-ALK lines were used to assess cytolytic capacity of ALK CAR T cells, and differences in cytolytic activity against ALK^{low} compared to ALK^{high} tumors were assessed by a two-way ANOVA followed by a Sidak's multiple comparisons test. (C) Cytokine production by ALK CAR T cells across a range of antigen densities was also assessed after a 24-hr co-incubation with NALM-6-GL-ALK cell lines, and curve fitting was done using a four-parameter variable slope dose-response curve. The gray shaded area indicates the range of endogenous ALK density found on neuroblastoma and Ewing sarcoma cell lines evaluated, and the dotted line indicates the ALK density that elicited half-maximum cytokine production (EC_{50}). (D) The amount of antigen required to elicit half-maximum production of IL-2, TNF-α, and IFN-γ was calculated for three independent experiments, and differences in the half-maximum threshold between cytokines was evaluated using a repeated-measures one-way ANOVA followed by a Dunnett's multiple comparisons test. EC_{50} values from the same experiment are indicated by matched symbols. (E) In vivo anti-tumor activity of the ALK CAR against ALK^{high} and ALK^{low} NALM-6-GL was assessed. Leukemia burden was monitored by imaging of luciferase activity. Tumor-free survival was calculated and significance evaluated by the log rank test (n = 5 mice per group). In vitro and in vivo data are representative of three experiments with different PBMC donors.

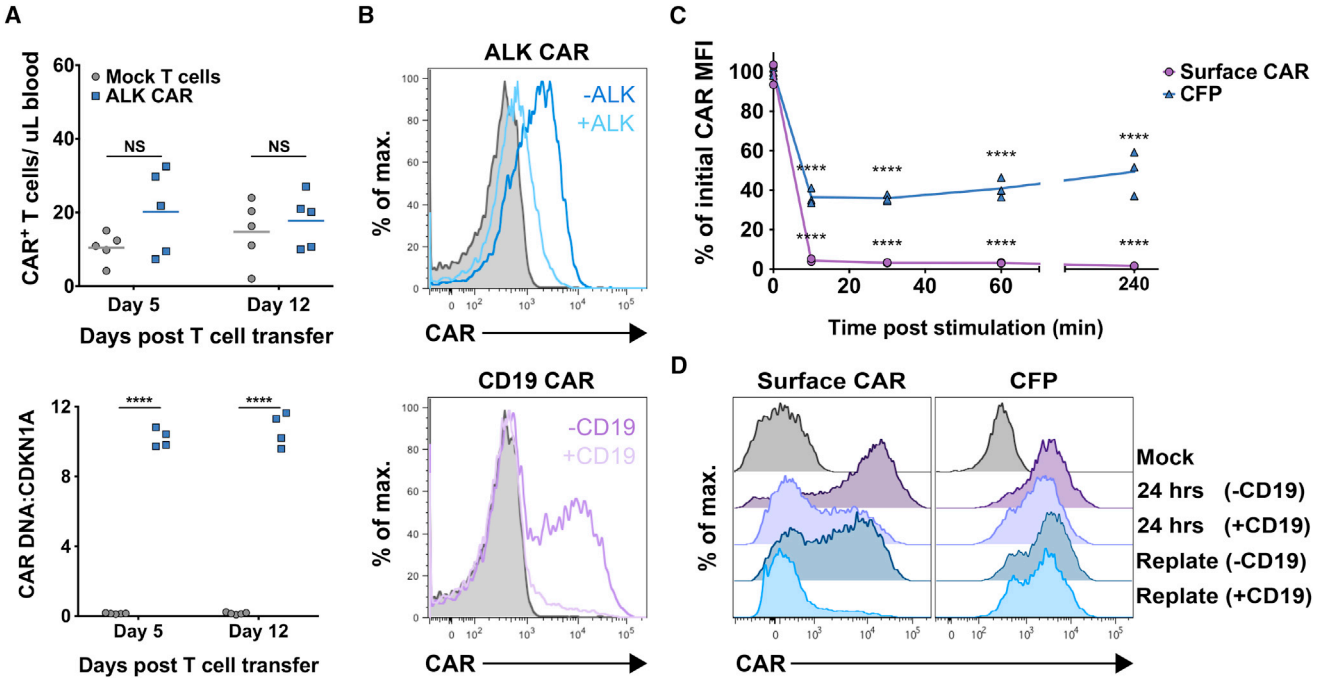

Figure 4. Down-Modulation of CAR Surface Expression after Antigen Encounter

CAR persistence was evaluated by flow cytometry from the peripheral blood of mice inoculated with NALM-6 ALK^{high} cells followed by ALK CAR T cells. (A) The number of surface CAR$^+$ T cells in the peripheral blood on day 5 and day 12 post T cell transfer are shown (top panel). CAR persistence was also evaluated by qPCR of genomic DNA isolated from peripheral blood (bottom panel). Differences in the number of T cells expressing surface CAR or CAR DNA compared to mock T cells were assessed by a repeated-measures two-way ANOVA followed by a Sidak's multiple comparison test. Flow cytometry data are representative of three in vivo experiments with different donors, and qPCR data were collected from one experiment at two time points. (B) ALK or CD19 CAR T cells were mixed 1:2 with CD19^{KO} NALM6-GL (ALK$^-$CD19$^-$) or NALM6-GL-ALK$^+$ (ALK$^+$CD19$^+$) tumor lines, and CAR expression was evaluated 5 hr later by flow cytometry. (C) Measures of surface CAR mean fluorescent intensity (MFI) and CFP MFI after antigen encounter are expressed as percentages of initial CAR/CFP expression. Differences from initial CAR expression at 0 min were determined by a repeated-measures two-way ANOVA followed by a Dunnett's multiple comparisons test. (D) T cells expressing a CD19 CAR-CFP fusion protein were exposed to CD19-expressing tumor for 24 hr, and then they were replated with or without tumor. T cells were evaluated for CAR surface expression and total CAR expression (CFP) by flow cytometry at 24 and 40 hr. Downregulation experiments were repeated three times with different PBMC donors.

CD19 CAR fused with CFP,[28] we further probed the kinetics of CAR down-modulation. Down-modulation of the CAR was rapid, as nearly all CAR disappeared from the T cell surface within 10 min of antigen encounter (Figure 4C). Total cellular CAR protein levels as measured by CFP fluorescence were partially diminished at this time point, but to a lesser extent than surface CAR.

To better study the dynamics CAR receptor loss, we co-incubated CD19 CAR-CFP T cells with CD19-positive tumor cells for 24 hr, and then we replated these cells either in media or again with antigen-positive tumor cells. As expected, surface CAR expression was markedly diminished after 24-hr incubation with CD19$^+$ tumor cells. However, total CAR protein levels as measured by CFP fluorescence remained comparatively high at this time point, indicating the presence of internalized CAR in T cells that had been exposed to antigen (Figure 4D). CAR T cells regained surface CAR expression after an additional 16-hr incubation in media, but surface CAR remained low in CAR T cells incubated again with CD19$^+$ tumor (Figure 4D). We attempted to replicate these experiments in the ALK CAR system, but fusion of the CFP protein to the ALK CAR completely abrogated ALK CAR expression, potentially due to an inherent inefficiency of expression with this construct. Nonetheless, we conclude that CAR down-modulation occurs at least in part due to receptor internalization.

CAR Expression Levels and Antigen Density Cooperate to Determine the Strength of CAR T Cell Activation

Based on the evidence that target density limits CAR T cell function (Figure 3), we reasoned that CAR expression level could similarly impact signal strength and limit CAR T cell function, especially since CARs are rapidly lost from the cell surface after antigen encounter. We therefore sought to simultaneously probe the impact of CAR density and antigen density on CAR signaling. Given the ability of protein L to bind to the extracellular scFv component of the ALK CAR, we titrated plate-bound Protein L to model variable target density. We first confirmed that Protein L stimulation largely replicated the findings seen using variable levels of cell-based target. Indeed, ALK CAR T cells required exposure to higher densities of cross-linking Protein

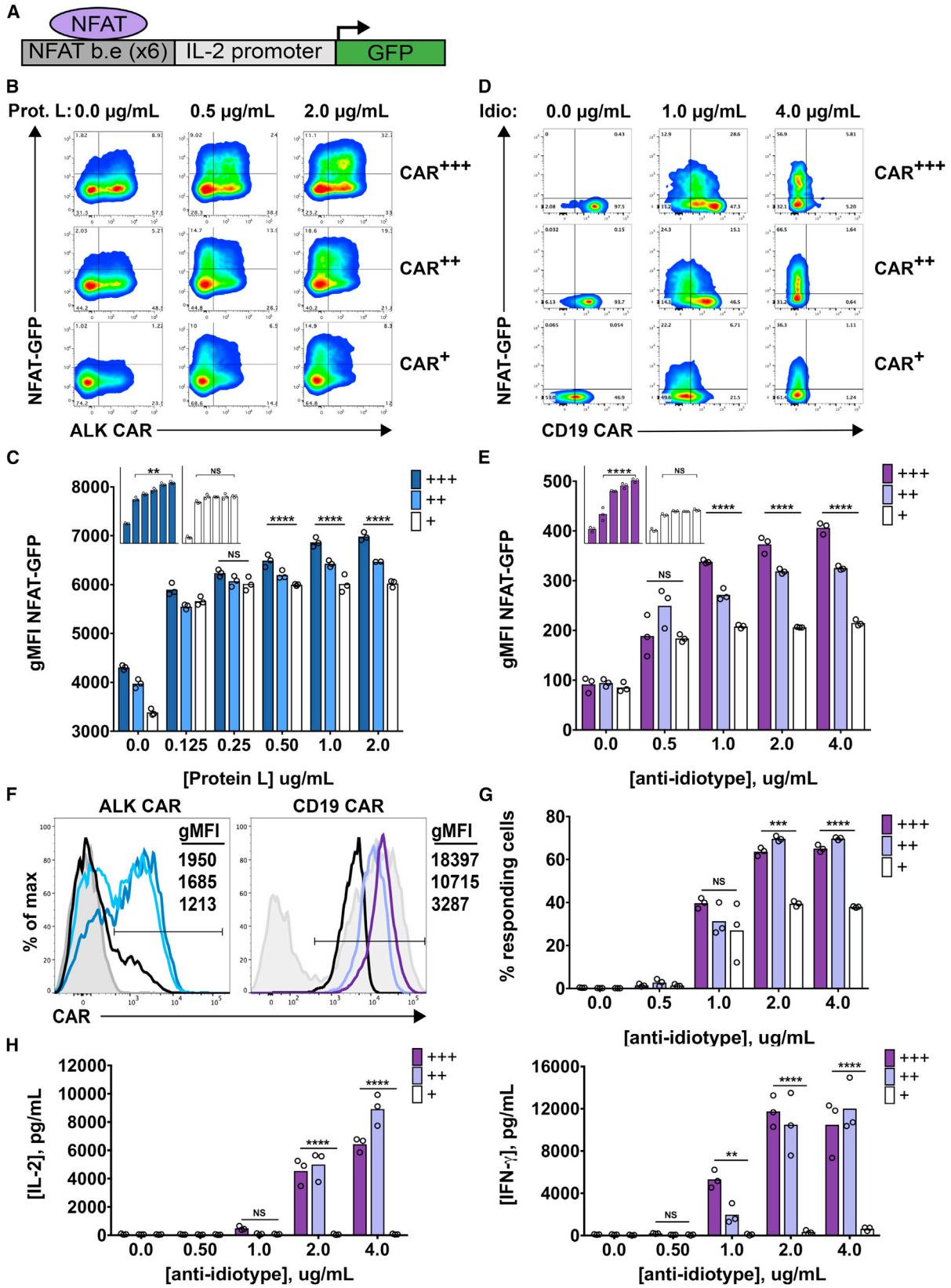

(legend on next page)

L to produce IL-2 compared to IFN-γ (Figure S3A). We next titrated the ALK CAR retroviral supernatant to achieve different levels of ALK CAR expression on T cells. We were able to modestly diminish cell surface CAR density by this method, and we also observed a decrease in the percentage of CAR$^+$ T cells when lower amounts of retroviral supernatant were used (Figure 5F). We then measured CAR T cell activation using an NFAT-inducible GFP reporter[31,32] following receptor cross-linking (Figure 5A). Induction of GFP expression by Protein L stimulation was specific to signaling through the CAR, as untransduced T cells did not increase GFP expression after stimulation with Protein L (Figures S3B and S3C). As shown in the representative contour plots and quantified data (Figures 5B and 5C), both target density and CAR density significantly influenced NFAT activity in ALK CAR T cells. When CAR density was high, increasing antigen density elicited an NFAT-GFP response of progressively higher magnitude. However, low CAR-expressing cells failed to elicit an increased response at higher antigen densities. Importantly, the intrinsic ability of low CAR-expressing T cells to activate the NFAT-GFP reporter was not impaired compared to medium and high CAR-expressing T cells, as demonstrated by a slightly higher NFAT-GFP response after stimulation with anti-CD3/CD28 beads (Figure S3D).

To determine whether this interaction between CAR density and antigen density is conserved across CARs, we repeated similar experiments with CD19.4-1BB.ζ-BFP CAR T cells and an NFAT-GFP reporter that also expressed truncated surface nerve growth factor receptor (NGFR) to allow for gating NFAT-GFP reporter-positive cells only. We sorted via fluorescence-activated cell sorting (FACS) the high, medium, and low CAR-expressing populations based on BFP expression, and we were able to achieve a broader and more pure range of CAR expression than seen in the ALK CAR T cells (Figure 5F). We stimulated these CD19 CAR T cells on plates coated with anti-(CD19 scFv)-idiotype antibody,[33] and we evaluated NFAT-GFP activity. Similarly to ALK CAR T cells, high CD19 CAR-expressing T cells showed an increased magnitude of response at higher antigen densities, whereas low CD19 CAR-expressing T cells rapidly reached a plateau of NFAT-GFP response (Figures 5D and 5E).

Since we were able to obtain pure populations of CAR$^+$/NFAT-GFP reporter$^+$ T cells by sorting the CD19 CAR and gating only on T cells expressing the truncated NGFR tag included in the NFAT-GFP reporter construct, we could also better assess the impact of CAR density and antigen density on recruitment of T cells into the responding (GFP$^+$) pool. The percentage of CD19 CAR T cells responding increased with antigen density. Additionally, while high- and medium-expressing populations of CD19 CAR T cells showed similar percentages of response at each antigen density, low-expressing CD19 CAR T cells showed a markedly lower percentage of cells responding, especially at high antigen densities (Figure 5G). This attenuated magnitude and penetrance of response by low-expressing CAR T cells was also reflected in the amount of IFN-γ and IL-2 produced by this cell population in response to antigen stimulation. Indeed, populations of low-expressing CD19 CAR T cells produced drastically reduced amounts of cytokines compared to medium- and high-expressing cells (Figure 5H). We conclude from these data that CAR surface density and target antigen density cooperate to regulate signal strength in CAR T cells. The impact of low CAR or low antigen density on the activation of CAR T cell effector functions is profound and conserved across the CARs we have examined.

DISCUSSION

Several recent studies have identified aberrant ALK activity as a driver of neuroblastoma transformation and growth,[5–7,34] and high ALK expression has been correlated with poor survival in patients with neuroblastoma.[10,11] Based on ALK overexpression in a majority of neuroblastoma patient samples and cell lines evaluated and a known role for ALK in oncogenesis,[6,8,34] we sought to develop a CAR targeting ALK. ALK surface protein expression on neuroblastoma cell lines was moderate and significantly increased above normal tissues, yet the ALK CAR showed limited in vivo anti-tumor activity. Using a library of NALM-6 B cell leukemia lines overexpressing ALK at different densities, we demonstrated a critical role for target antigen density in limiting CAR efficacy, in agreement with previous reports showing impaired CAR T cell lytic capacity at low antigen densities.[35–42]

Figure 5. Regulation of CAR T Cell Activity by CAR Density and Antigen Density

A GFP reporter system indicating NFAT activity was used to evaluate CAR T cell activation upon receptor cross-linking with plate-bound Protein L or anti-(CD19 scFv)-idiotype antibody. (A) The lentiviral construct incorporates six NFAT-binding elements upstream of a minimal IL-2 promoter, and it drives GFP expression upon T cell activation. (B) ALK CAR/NFAT-GFP reporter T cells were spun onto 96-well plates coated with biotinylated Protein-L concentrations as shown, and they were assessed by flow cytometry 24 hr later for surface CAR and GFP expression. Representative plots of NFAT-GFP activity in populations of T cells with low initial CAR expression (CAR$^+$), medium initial CAR expression (CAR^{++}), and high initial CAR expression (CAR^{+++}) are indicated. (C) Geometric mean fluorescent intensity (gMFI) of NFAT-driven GFP expression was quantified in the GFP-positive population of responding cells. Insets are visual comparisons of the NFAT response to increasing antigen density by high- (+++, blue) and low- (+, white) expressing ALK CAR T cells. (D and E) CD19.4-1BB. ζ-BFP/NFAT-GFP reporter CAR T cells were spun onto 96-well plates coated with varying concentrations of anti-(CD19 scFv)-idiotype antibody, and they were assessed by flow cytometry 24 hr later for surface CAR and GFP expression. Representative plots of NFAT-GFP activity in populations of T cells with low initial CAR expression (CAR$^+$), medium initial CAR expression (CAR^{++}), and high initial CAR expression (CAR^{+++}) are indicated (D) and quantified (E). (F) Representative FACS plots of CAR expression and gMFI are shown for ALK CARs and sorted CD19 CARs used in the NFAT-GFP reporter assays. For the ALK CAR: dark blue, high (+++) CAR; light blue, medium (++) CAR; black, low (+) CAR; gray shaded, mock. For the CD19 CAR: dark purple, high (+++) CAR; light purple, medium (++) CAR; black, low (+) CAR; gray shaded, unsorted CAR-transduced population. (G) The percentage of CD19 CAR T cells (NFAT-GFP$^+$ cells) responding to anti-idiotype stimulation is shown. (H) IFN-γ and IL-2 production was assessed after co-incubation of sorted CD19 CAR T cells with varying concentrations of plate-bound anti-idiotype antibody. Differences in the gMFI of GFP, percentage of CARs responding, and cytokines produced were determined by a two-way ANOVA followed by a Tukey's multiple comparisons test. Experiments were repeated three times with a total of two different donors.

Production of IL-2, TNF-α, and IFN-γ by stimulated ALK CAR T cells revealed a sharp threshold, with appreciable cytokine production occurring only above the upper limit of ALK expression observed on neuroblastoma cell lines. Cytokine production thresholds have also been demonstrated for CAR T cells targeting CD20 and CD30 antigens.[40,41] With the ALK CAR, there was a significantly higher threshold for IL-2 production compared to IFN-γ, which parallels data showing hierarchical cytokine production for T cells stimulated through the native T cell receptor (TCR).[43] These antigen-dependent differences in cytolytic activity and cytokine production by ALK CAR T cells correlated with in vivo anti-tumor efficacy. Thus, antigen density governs several aspects of ALK CAR T cell function, and it has a substantial impact on the efficacy of CAR T cell anti-tumor responses in vivo. This differential response of CAR T cells to low and high antigen density may allow for the exploitation of a therapeutic window in which a low level of tumor antigen expression on normal tissue can be tolerated when targeting a tumor with high expression of the antigen.

We also sought to determine whether modulation of CAR density influences the efficacy of CAR T cell therapy. Activation of ALK CAR T cells or CD19 CAR T cells expressing a low density of surface receptor was severely impaired compared to T cells expressing a high density of receptor, especially at high antigen densities. These findings suggest that an interaction between CAR density and antigen density regulates T cell potency. Previous studies report impairment of cytolytic capacity and cytokine production at low CAR and low antigen densities.[35,36,44,45] Our data additionally suggest that differences in these population-based measures of T cell function are driven by both the magnitude of response by individual CAR T cells and by the proportion of responding cells across the population of CAR T cells. This result in part contrasts with recent reports of digital cytokine production by T cells stimulated through the native TCR, where an increase in the density of peptide-MHC presented led to an increase in the number of T cells producing IL-2 and TNF-α, but not to an increase in the magnitude of cytokine production by individual T cells.[46] This discrepancy could result from differences in methodology used to address this question or, more intriguingly, from fundamental differences in the regulation of signaling through the native TCR versus through engineered CAR receptors.[47]

Our data indicate that strategies to manipulate tumor antigen and/or CAR density could allow fine-tuning of CAR T cell activity. Modulation of antigen density is an emerging possibility due to techniques aimed at epigenetic modification of tumor gene expression.[48,49] Target expression may also be amenable to regulation by other classes of small molecule therapeutics. For example, the inhibition of ALK signaling by the tyrosine kinase inhibitor Crizotinib leads to upregulation of ALK surface expression,[24] providing an opportunity for rational co-therapy. CAR density could be regulated by the alteration of promoter strength, and it could additionally be controlled at the transcriptional, translational, or post-translational level. A final strategy to augment the interaction between CAR receptors and tumor antigen could include alteration of CAR affinity, as has been demonstrated by several recent studies.[39,50] An affinity-enhanced ALK CAR could allow for targeting of pediatric tumors with low to intermediate expression of ALK by stabilizing T cell-tumor interactions in the absence of high-density receptor-antigen binding. A more precise mathematical modeling of the tripartite relationship among CAR affinity, CAR density, and antigen density, with regard to activation of T cell effector functions, would be informative, since simultaneous tuning of these parameters has the potential to enhance anti-tumor activity while minimizing on-target, off-tumor toxicities.

We also discovered that ALK CAR and CD19 CAR T cells showed nearly complete CAR down-modulation upon co-incubation with tumors expressing high levels of cognate antigen. These data agree with previous studies of first-generation CARs targeting CD20 and CD22,[37,45] as well as second-generation CARs targeting HER-2 and C4 folate receptor-alpha.[51,52] CAR down-modulation seems to be well conserved across scFvs and co-stimulatory domains. To more carefully study CAR down-modulation, we took advantage of a CAR construct comprising the CD19.4-1BB.ζ CAR tagged with CFP.[28] The CD19.4-1BB.ζ-CFP CAR showed rapid down-modulation that was enforced by constitutive antigen contact in vitro. CARs re-expressed on the cell surface upon the removal of antigen, consistent with CAR cycling to the cell surface after initial CAR T cell contact with antigen. Similarly, native TCRs recycle to the cell surface after initial antigen encounter,[53,54] and they contribute to the sustained TCR signaling that is required for full activation of T cell cytokine production and proliferation.[46,55–58] We further demonstrated that significant CAR down-modulation occurred in vivo. As reported previously, down-modulation may also occur as a result of epigenetic silencing of the retroviral construct used to introduce the CAR.[59]

Regardless of the mechanism, the question remains as to how CAR down-modulation contributes to the outcome of the CAR T cell anti-tumor response. Regrettably, we were not able to inhibit CAR down-modulation in this model system to answer this question definitively. However, based on our data regarding the detrimental impact of low CAR density on CAR T cell function, we propose that CAR down-modulation could regulate CAR T cell activation by limiting the number of receptors available to sustain downstream signaling after initial antigen encounter. For CARs that initially express at lower levels like the ALK CAR, down-modulation may lead to diminished efficacy because ligation of this small number of receptors is insufficient to allow the cell to reach a threshold required for the activation of effector functions. Conversely, CARs that express high levels of receptor like the CD19 CAR might benefit from CAR down-modulation, as it could limit hyper-activation and exhaustion of the T cell that results from repetitive antigen stimulation. It is important to note for future CAR development that receptors that do not express at sufficient levels may be functionally impaired, even when tumor antigen is expressed at a moderate to high level.

In summary, we demonstrate that CAR T cell function can be limited by both CAR receptor density and target antigen density. Unlike

native T cells, which are known to signal through the TCR in response to very low antigen density, the engineered CAR T cells studied here require much higher antigen densities to fully activate effector functions. This work leads to the prediction that selection of tumor variants with low-level antigen expression may prove to be an Achilles' heel for CAR T cell therapy, as has been previously observed with CD19 CAR T cells and now with CD22 CAR T cells as well (T.J.F., N.N. Shah, R.J.O., H. Qin, M. Stetler-Stevenson, C.M. Yuan, P. Wolters, S. Peron-Martin, S. Ramakrishna, C. Delbrook, B. Yates, H. Shalabi, R.G. Majzner, D.F. Stroncek, M. Sabatino, Y. Feng, D.S. Dimitrov, L. Zhang, S.M.N., B. Dropulic, D.W. Lee, and C.L.M., unpublished data). Furthermore, this work has important implications for tumor target selection. High absolute antigen expression appears to be a prerequisite for effective CAR therapeutics, and, as a corollary, low expression of target antigen on normal tissues may be tolerable in some circumstances. This understanding could broaden the range of tumor-associated antigens exploited for CAR T cell therapy, especially for solid tumors where the selection of antigens that are completely absent on normal tissue has been challenging. Future work is needed to more fully understand the factors responsible for a high-density antigen requirement for CAR T cells and to further explore the impact of manipulating CAR receptor down-modulation on CAR T cell function.

MATERIALS AND METHODS

Mice

Immunodeficient NSG mice (NOD.Cg-Prkdc^{scid} Il2rg^{tm1Wjl} /SzJ) were purchased from The Jackson Laboratory or bred in house. Mice used for in vivo experiments were between 6 and 12 weeks old, and the ratio of male to female mice was matched in experimental and control groups. All animal studies were carried out according to NCI Animal Care and Use Committee-approved protocols.

Cells and Culture Conditions

Human cell lines used in these studies were supplied by the following sources: SH-SY5Y, LAN5, K562, and CHP-100 by C. Thiele (NCI, NIH); Kelly by Sigma-Aldrich (92110411); EW8 by L. Helman (NCI, NIH); 143B by C. Khanna (NCI, NIH); NALM-6-GL by S. Grupp (University of Pennsylvania); and 293GP and 293T by the Surgery Branch (NCI, NIH). A short tandem repeat (STR) DNA analysis (DDC Medical) was conducted to verify the identity of all cell lines, and each cell line was validated to be *Mycoplasma* free by qPCR. The 293GP and 293T cell lines were cultured in DMEM. All other cells were cultured in RPMI-1640. DMEM and RPMI-1640 media were supplemented with 2 mM L-glutamine, 10 mM HEPES, 100 U/mL penicillin, 100 μg/mL streptomycin (Invitrogen), and 10% heat-inactivated fetal bovine serum (FBS; Gemini Bioproducts).

Elutriated human peripheral blood mononuclear cells (PBMCs) from consenting, healthy donors were obtained from the Department of Transfusion Medicine, NIH Clinical Center, under an NIH IRB-approved protocol, and cryopreserved. Thawed PBMCs were cultured in AIM-V media (Invitrogen) supplemented with 2 mM L-glutamine, 10 mM HEPES, 100 U/mL penicillin, 100 μg/mL streptomycin, 5% heat inactivated FBS, and r-human IL-2 (aldesleukin, Prometheus).

ALK CAR Construct Synthesis

To sequence the variable regions of ALK48 heavy and light chains, PCR primers were used to amplify hybridoma cell line-derived cDNA. PCR primer sequences specific for murine IgG were obtained from Kettleborough et al.[60] Frozen hybridoma cell pellets were resuspended in RLT buffer and passed over QIAShredder columns, and total RNA was isolated on RNAeasy spin columns (QIAGEN), following the manufacturer's protocol. PCR products were cloned into a TopoTA vector (Invitrogen), and ten independent bacterial colonies were DNA sequenced. Sequence runs for heavy and light chains were aligned, consensus was determined, and cognate heavy and light chains were linked with a (GGGGS)×3 sequence to create an scFv sequence. ALK scFv-encoding plasmids were sequence optimized and synthesized by DNA2.0, and then they were introduced into an MSGV.1 retroviral expression vector containing a CD8-α transmembrane domain, a CD137 (4-1BB) co-stimulatory motif, and a CD3ζ signaling domain, or a CD28 transmembrane and co-stimulatory motif and a CD3ζ signaling domain as previously described.[29] Where indicated, the sequence of the human IgG1 constant domain (CH2-CH3) was inserted between the scFv and the transmembrane domain. Resultant ALK CAR constructs were sequence verified (Macrogen USA) and used for downstream applications.

CAR T Cell Transduction

Retroviral supernatant for the ALK CARs or other CD19 CARs (MSGV.CD19.4-1BB.ζ, MSGV.CD19.4-1BB.ζ.CFP, and MSGV.CD19.4-1BB.ζ-BFP)[28] was produced by transient transfection of 293GP cells with the corresponding CAR plasmid and an RD114 envelope plasmid. Lentiviral supernatant carrying the NFAT-inducible GFP vector (courtesy of Dr. Richard Morgan, NCI-Surgery Branch) or NFAT-GFP/truncated NGFR vector was produced by transient transfection of 293T cells with a third-generation transfer plasmid and packaging plasmids RRE, pMD-G, and REV. PBMCs were thawed and activated by culture for 2 or 3 days in the presence of 40 U/mL rhIL-2 and anti-CD3/CD28 beads (Dynabeads, Human T-Activator CD3/CD28, Life Technologies) at a 3:1 bead:T cell ratio. Cells were exposed to RV-containing supernatants on days 2 and 3, or days 3 and 4, in media containing 300 U/mL rIL-2 on retronectin-coated non-tissue culture plates (on plate method as per manufacturer, Takara/Clonetech). Beads were magnetically removed on day 4 or 5, and cells expanded in AIM-V media containing 300 U/mL IL-2 until use in vitro and in vivo. For experiments using the NFAT-inducible GFP reporter, bead-activated PBMCs were transduced on day 1 with NFAT-GFP lentiviral supernatant and then on days 2 and 3 with CAR retroviral supernatant on retronectin-coated plates, and they expanded as described above. For most assays, CAR T cells were used on day 2–5 post bead removal.

Lentiviral Engineering of Tumor Cell Lines

NALM-6-GL cell lines stably overexpressing ALK were produced by lentiviral transduction with supernatant (produced as described

above) containing a third-generation vector encoding the extracellular and transmembrane domains of ALK. The resultant bulk population was stained using ALK48 antibody and sorted into high-, medium-, and low-expressing lines on a FACS Aria (BD Biosciences). The bulk populations were then single-cell cloned on 96-well plates to create clones with distinct levels of ALK expression.

The CD19 knockout NALM-6-GL cell line was produced using CRISPR/Cas9 technology. Briefly, guide RNAs were designed from the GeCKO human single-guide RNA (sgRNA) library, cloned into a LentiCRISPR v2 plasmid (plasmid 52961, Addgene), and transformed as previously described.[61] Guide RNA sequences were as follows: hCD19F: 5′CACCGTGGAATGTTTCGGACCTAGG 3′ and hCD19R: 5′ AAACCCTAGGTCCGAAACATTCCAC 3′. CRISPR vector and packaging plasmids RRE, pMD-G, and REV were co-transfected into LentiX HEK293T cells (Clontech). Viral supernatants were collected and concentrated using a Lenti-X concentrator (Clontech). After transduction, CD19 expression was assessed by flow cytometry and $CD19^-$ cells were sorted for single-cell cloning. DNA from clones was amplified using the Plantinum PCR Supermix High Fidelity Kit (Invitrogen) and verified by sequencing (Macrogen USA).

T Cell Functional Assays

T cell cytolytic function was assayed in standard ^{51}Cr-release assays as described elsewhere.[29] Cytokine release was assayed by co-incubating 25,000 or 100,000 T cells with 25,000 or 100,000 tumor cell targets in complete RPMI-1640 (composition described above). At 24 hr, culture media were collected and cytokines were measured by a Human TH1/TH2 multiplex assay (Meso Scale Discovery).

Antibodies and Flow Cytometry Analyses

The ALK48 antibody was a generous gift from Dr. Marc Vigny. Additional ALK48 antibody was produced by the Frederick National Laboratory Protein Expression Laboratory (NIH, NCI) by expressing the antibody heavy- and light-chain sequences in HEK293e cells and purification of supernatant on a Protein A column. The ALK48 antibody was conjugated using a Dylight 650 Antibody Labeling Kit (Thermo Fisher Scientific). Staining for ALK expression on tumor lines was performed using methods described above, and ALK expression was quantified using the same antibody with the Quantum Simply Cellular kit[62] (Bangs Laboratories).

CAR expression on transduced T cells was also measured by flow cytometry. CAR T cells were stained with Biotin-Protein L (Thermo Fisher Scientific), followed by fluorophore-conjugated streptavidin (BD Biosciences) and anti-human CD3ε (clone OKT3, eBioscience). In some cases, CD19 CARs were stained using an anti-(CD19scFv)-idiotype antibody provided by L.J. Cooper (MD Anderson).[33] For in vivo experiments, CAR T cells were identified in the peripheral blood of recipient mice using anti-human CD45 (clone H130, eBioscience), anti-human CD3ε (clone OKT3, eBioscience), and Biotin-Protein L and fluorophore-conjugated streptavidin. All staining was performed in 0.1 mL FACS buffer (PBS + 2% BSA + 2 mM EDTA). Live single T cells were identified by forward scatter and side scatter parameters and additional staining with Fixable Viability Dye eFluor 506 (eBioscience). Flow cytometry was performed using a FACS Fortessa (BD Biosciences) and analyzed with FlowJo software (Tree Star).

Microarray Data for *ALK* Expression

Microarray data for *ALK* RNA expression was accessed through the Pediatric Tumor Affymetrix Database (NCI Pediatric Oncology Branch, https://home.ccr.cancer.gov/oncology/oncogenomics). This database includes expression data for an array of pediatric tumor cell lines, patient-derived xenografts, and tumor biopsies. Log fold change values were calculated relative to mean *ALK* expression in a normal tissue array included in the dataset.

Tumor Models and CAR T Cell Therapy

Animal studies were carried out under protocols approved by the NCI Bethesda Animal Care and Use Committee. The Kelly and SY5Y cell lines were expanded under standard culture conditions (described above) and harvested with 2 mM EDTA (KD Medical) in PBS (Gibco, Thermo Fisher Scientific). Cells were washed twice in cold PBS and resuspended in a 1:1 mixture of PBS and Growth Factor Reduced Matrigel (356231, Corning). NSG Mice were inoculated subcutaneously on the right flank with 1.0×10^6 (Kelly) or 2.0×10^6 (SY5Y) tumor cells in 0.1 mL total volume with a sterile 25-gauge needle. Two days after inoculation, treatment groups were injected intraperitoneally (i.p.) with 2.0 mg Cyclophosphamide in 0.2 mL PBS (EMD Biosciences). ALK CAR-bearing T cells (1.5×10^7 CAR-positive cells or an equivalent total number of mock-transduced cells in PBS per mouse) were transferred by tail vein injection (intravenously [i.v.]) on day 3 or day 5 after tumor inoculation. Mice received i.p. injections of 1.0 μg recombinant human (rh) IL-7 (Cytheris) and 5.0 μg M25 (anti-IL-7 antibody, Immunex/Amgen) in 0.2 mL PBS three times per week following T cell transfer. Tumor growth was measured with digital calipers, and area was calculated by multiplying the length of the major and minor axes of each tumor.

For studies involving NALM-6-GL-ALK tumors, 1×10^6 tumor cells were transferred to NSG mice by tail vein injection. Three days later, 1×10^7 ALK CAR^+ T cells or an equivalent total number of mock-transduced T cells were transferred intravenously. NALM6-GL leukemia burden was evaluated using the Xenogen IVIS Lumina (Caliper Life Sciences). Mice were injected i.p. with 3 mg D-luciferin (Caliper Life Sciences) and then imaged 4 min later with an exposure time of 30 s. Luminescence images were analyzed using Living Image software (Caliper Life Sciences). Mice were considered tumor free if they did not show luciferase signal at any point during the course of treatment. Mice that died with symptoms of graft versus host disease but undetectable tumor burden were censored in the log rank survival analysis.

NFAT-GFP T Cell Activation Assay

NFAT activity downstream of CAR activity was assessed after cross-linking of CARs by plate-bound Protein L or anti-(CD19

scFv)-idiotype antibody. 96-well ELISA microplates were coated with varying concentrations of Biotin-Protein L (0.0–2.0 μg/mL) or anti-idiotype antibody (0.0–4.0 μg/mL) in PBS overnight at 4°C. Plates were washed three times with PBS and allowed to dry before use. Varying levels of surface CAR expression for the ALK CAR were achieved by transducing T cells with different concentrations of ALK48.4-1BB-ζ supernatant after NFAT-GFP reporter transduction. Varying levels of CD19 CAR were achieved by FACS of T cells co-transduced with CD19.4-1BB.ζ-BFP supernatant and NFAT-GFP/tNGFR supernatant based on varied BFP expression. CAR or Mock T cells co-transduced with an NFAT-inducible GFP reporter were spun onto coated plates in triplicate (200,000 cells in 200 μL AIM-5/well) at 100 × *g* for 1 min, and they were incubated at 37°C for 24 hr. As a control for maximum NFAT activation, separate groups of CAR or Mock T cells were also mixed at a 1:1 ratio with anti-CD3/CD28 beads and spun onto PBS-coated wells. T cells were harvested from wells and transferred to a round-bottom 96-well plate for subsequent staining and analysis by flow cytometry. For the ALK CAR, the magnitude of NFAT activity at varying antigen and CAR densities was calculated as the geometric mean fluorescent intensity of GFP^+ T cells. For the CD19-BFP CAR, cells containing the NFAT-GFP reporter construct were first identified by gating on T cells co-expressing the tNGFR tag. Then, the magnitude of NFAT activity was calculated as the geometric mean fluorescent intensity of GFP^+ cells, and the percentage of responding cells was calculated as the percentage of GFP^+ cells out of total cells.

CAR Down-Modulation Assays

Antigen-dependent CAR T cell down-modulation was assessed by co-incubating ALK CAR, CD19 CAR, CD19-CFP CAR, or CD19-BFP CAR T cells at a 1:2 T cell:tumor ratio with NALM-6-GL-ALK cells ($CD19^{hi}ALK^{hi}$) or isogenic NALM-6-GL-$CD19^{KO}$ cells ($CD19^-ALK^-$) (created by CRISPR-mediated knockout). T cells were mixed with tumors, centrifuged for 1 min at 100 × *g*, incubated at 37°C, and harvested into ice-cold FACS buffer containing 0.1% sodium azide at various time points. CAR surface expression and CFP fluorescence were assessed by flow cytometry at different time points between 0 and 6 hr after antigen contact. To study the dynamics of CAR recycling after antigen encounter, we seeded CD19-CFP CAR T cells into six-well plates containing a monolayer of adherent $CD19^+$ 143B tumor cells.[28] After a 24-hr co-incubation, CAR T cells were harvested and transferred to a new plate either containing $CD19^+$ 143B cells or media. After an additional 16-hr incubation, CAR surface expression and CFP expression were determined as described above.

Real-Time PCR for CAR T Cell Persistence

Peripheral blood (50 μL) was harvested by retro-orbital bleed into heparinized tubes, and genomic DNA was harvested with the DNeasy Blood and Tissue Kit (QIAGEN). Total gDNA was assayed for CAR expression by qPCR using TaqMan Fast Universal PCR Master Mix (Applied Biosystems) on an Applied Biosystems StepOnePlus real-time PCR machine. The following TaqMan primers (Applied Biosystems) were used: a probe targeting the 4-1BB:CD3ζ junction of the CAR construct (*CDTMBB*; assay ID AJBJXJ0) and cyclin-dependent kinase inhibitor 1 (*CDKN1A*; assay ID AIQJCFT). Relative CAR persistence was calculated by normalizing CAR signal to *CDKN1A* DNA.

Graphs and Statistical Analysis

Data were visualized and analyzed using GraphPad Prism software. Graphs represent either group mean values ± SEM or individual values. The p values were calculated using the following: one or two-way ANOVAs followed by appropriate post hoc tests reflecting multiple comparisons (details indicated in the figure legends); the repeated-measures ANOVA for tumor growth curves; and log rank statistics for survival analyses. $p < 0.05$ was considered statistically significant, and p values are denoted with asterisks as follows: $p > 0.05$, not significant, NS; *$p < 0.05$, **$p < 0.01$, ***$p < 0.001$, and ****$p < 0.0001$.

SUPPLEMENTAL INFORMATION

Supplemental Information includes three figures and can be found with this article online at http://dx.doi.org/10.1016/j.ymthe.2017.06.008.

AUTHOR CONTRIBUTIONS

A.J.W., R.G.M., R.J.O., and C.L.M. conceived of the study, and A.J.W., R.G.M., and C.L.M. wrote and revised the manuscript. A.J.W. and R.G.M. conducted the majority of in vitro and in vivo experiments. M.V. developed and provided the ALK48 antibody used to design the ALK CAR. P.L. sequenced and constructed ALK CAR vectors and conducted initial experiments demonstrating feasibility of ALK CAR T cell therapy. S.M.N. and T.J.F. created and validated the transgenic cell lines used. L.Z., A.H.L., and K.W. designed and validated other constructs used throughout the paper.

CONFLICTS OF INTEREST

C.L.M. and R.J.O. hold a patent comprising use of the ALK CARs for cancer immunotherapy. The other authors have no conflicts to disclose.

ACKNOWLEDGMENTS

This research was supported by the Intramural Research Program of the NIH, CCR, NCI. Research was also supported by a Stand Up To Cancer - St. Baldrick's Pediatric Dream Team Translational Research Grant (SU2C-AACR-DT1113). Stand Up To Cancer is a program of the Entertainment Industry Foundation administered by the American Association for Cancer Research. C.L.M. is a member of the Parker Institute for Cancer Immunotherapy, which supports the Stanford University Cancer Immunotherapy Program. We would also like to thank John Buckley and Jabril Johnson for technical assistance.

REFERENCES

1. Palmer, R.H., Vernersson, E., Grabbe, C., and Hallberg, B. (2009). Anaplastic lymphoma kinase: signalling in development and disease. Biochem. J. *420*, 345–361.

2. Morris, S.W., Kirstein, M.N., Valentine, M.B., Dittmer, K.G., Shapiro, D.N., Saltman, D.L., and Look, A.T. (1994). Fusion of a kinase gene, ALK, to a nucleolar protein gene, NPM, in non-Hodgkin's lymphoma. Science *263*, 1281–1284.

3. Sasaki, T., Rodig, S.J., Chirieac, L.R., and Jänne, P.A. (2010). The biology and treatment of EML4-ALK non-small cell lung cancer. Eur. J. Cancer *46*, 1773–1780.
4. Chiarle, R., Voena, C., Ambrogio, C., Piva, R., and Inghirami, G. (2008). The anaplastic lymphoma kinase in the pathogenesis of cancer. Nat. Rev. Cancer *8*, 11–23.
5. Mossé, Y.P., Laudenslager, M., Longo, L., Cole, K.A., Wood, A., Attiyeh, E.F., Laquaglia, M.J., Sennett, R., Lynch, J.E., Perri, P., et al. (2008). Identification of ALK as a major familial neuroblastoma predisposition gene. Nature *455*, 930–935.
6. George, R.E., Sanda, T., Hanna, M., Fröhling, S., Luther, W., 2nd, Zhang, J., Ahn, Y., Zhou, W., London, W.B., McGrady, P., et al. (2008). Activating mutations in ALK provide a therapeutic target in neuroblastoma. Nature *455*, 975–978.
7. Chen, Y., Takita, J., Choi, Y.L., Kato, M., Ohira, M., Sanada, M., Wang, L., Soda, M., Kikuchi, A., Igarashi, T., et al. (2008). Oncogenic mutations of ALK kinase in neuroblastoma. Nature *455*, 971–974.
8. Heukamp, L.C., Thor, T., Schramm, A., De Preter, K., Kumps, C., De Wilde, B., Odersky, A., Peifer, M., Lindner, S., Spruessel, A., et al. (2012). Targeted expression of mutated ALK induces neuroblastoma in transgenic mice. Sci. Transl. Med. *4*, 141ra91.
9. Zhu, S., Lee, J.S., Guo, F., Shin, J., Perez-Atayde, A.R., Kutok, J.L., Rodig, S.J., Neuberg, D.S., Helman, D., Feng, H., et al. (2012). Activated ALK collaborates with MYCN in neuroblastoma pathogenesis. Cancer Cell *21*, 362–373.
10. Passoni, L., Longo, L., Collini, P., Coluccia, A.M., Bozzi, F., Podda, M., Gregorio, A., Gambini, C., Garaventa, A., Pistoia, V., et al. (2009). Mutation-independent anaplastic lymphoma kinase overexpression in poor prognosis neuroblastoma patients. Cancer Res. *69*, 7338–7346.
11. Schulte, J.H., Bachmann, H.S., Brockmeyer, B., Depreter, K., Oberthür, A., Ackermann, S., Kahlert, Y., Pajtler, K., Theissen, J., Westermann, F., et al. (2011). High ALK receptor tyrosine kinase expression supersedes ALK mutation as a determining factor of an unfavorable phenotype in primary neuroblastoma. Clin. Cancer Res. *17*, 5082–5092.
12. Mossé, Y.P. (2016). Anaplastic Lymphoma Kinase as a Cancer Target in Pediatric Malignancies. Clin. Cancer Res. *22*, 546–552.
13. Brentjens, R.J., Rivière, I., Park, J.H., Davila, M.L., Wang, X., Stefanski, J., Taylor, C., Yeh, R., Bartido, S., Borquez-Ojeda, O., et al. (2011). Safety and persistence of adoptively transferred autologous CD19-targeted T cells in patients with relapsed or chemotherapy refractory B-cell leukemias. Blood *118*, 4817–4828.
14. Brentjens, R.J., Davila, M.L., Riviere, I., Park, J., Wang, X., Cowell, L.G., Bartido, S., Stefanski, J., Taylor, C., Olszewska, M., et al. (2013). CD19-targeted T cells rapidly induce molecular remissions in adults with chemotherapy-refractory acute lymphoblastic leukemia. Sci. Transl. Med. *5*, 177ra38.
15. Grupp, S.A., Kalos, M., Barrett, D., Aplenc, R., Porter, D.L., Rheingold, S.R., Teachey, D.T., Chew, A., Hauck, B., Wright, J.F., et al. (2013). Chimeric antigen receptor-modified T cells for acute lymphoid leukemia. N. Engl. J. Med. *368*, 1509–1518.
16. Lee, D.W., Shah, N.N., Stetler-Stevenson, M., Sabatino, M., Delbrook, C., Richards, K., Kochenderfer, J.N., Rosenberg, S.A., Stroncek, D., Wayne, A.S., and Mackall, C.L. (2013). Anti-CD19 chimeric antigen receptor (CAR) T cells produce complete responses with acceptable toxicity but without chronic B-cell aplasia in children with relapsed or refractory acute lymphoblastic leukemia (ALL) even after allogeneic hematopoietic stem cell transplantation (HSCT). Blood *122*, 68.
17. Maude, S.L., Frey, N., Shaw, P.A., Aplenc, R., Barrett, D.M., Bunin, N.J., Chew, A., Gonzalez, V.E., Zheng, Z., Lacey, S.F., et al. (2014). Chimeric antigen receptor T cells for sustained remissions in leukemia. N. Engl. J. Med. *371*, 1507–1517.
18. Davila, M.L., Riviere, I., Wang, X., Bartido, S., Park, J., Curran, K., Chung, S.S., Stefanski, J., Borquez-Ojeda, O., Olszewska, M., et al. (2014). Efficacy and toxicity management of 19-28z CAR T cell therapy in B cell acute lymphoblastic leukemia. Sci. Transl. Med. *6*, 224ra25.
19. Lee, D.W., Kochenderfer, J.N., Stetler-Stevenson, M., Cui, Y.K., Delbrook, C., Feldman, S.A., Fry, T.J., Orentas, R., Sabatino, M., Shah, N.N., et al. (2015). T cells expressing CD19 chimeric antigen receptors for acute lymphoblastic leukaemia in children and young adults: a phase 1 dose-escalation trial. Lancet *385*, 517–528.
20. Ahmed, N., Brawley, V.S., Hegde, M., Robertson, C., Ghazi, A., Gerken, C., Liu, E., Dakhova, O., Ashoori, A., Corder, A., et al. (2015). Human Epidermal Growth Factor Receptor 2 (HER2)-Specific Chimeric Antigen Receptor-Modified T Cells for the Immunotherapy of HER2-Positive Sarcoma. J. Clin. Oncol. *33*, 1688–1696.
21. Louis, C.U., Savoldo, B., Dotti, G., Pule, M., Yvon, E., Myers, G.D., Rossig, C., Russell, H.V., Diouf, O., Liu, E., et al. (2011). Antitumor activity and long-term fate of chimeric antigen receptor-positive T cells in patients with neuroblastoma. Blood *118*, 6050–6056.
22. Pule, M.A., Savoldo, B., Myers, G.D., Rossig, C., Russell, H.V., Dotti, G., Huls, M.H., Liu, E., Gee, A.P., Mei, Z., et al. (2008). Virus-specific T cells engineered to coexpress tumor-specific receptors: persistence and antitumor activity in individuals with neuroblastoma. Nat. Med. *14*, 1264–1270.
23. Moog-Lutz, C., Degoutin, J., Gouzi, J.Y., Frobert, Y., Brunet-de Carvalho, N., Bureau, J., Créminon, C., and Vigny, M. (2005). Activation and inhibition of anaplastic lymphoma kinase receptor tyrosine kinase by monoclonal antibodies and absence of agonist activity of pleiotrophin. J. Biol. Chem. *280*, 26039–26048.
24. Carpenter, E.L., Haglund, E.A., Mace, E.M., Deng, D., Martinez, D., Wood, A.C., Chow, A.K., Weiser, D.A., Belcastro, L.T., Winter, C., et al. (2012). Antibody targeting of anaplastic lymphoma kinase induces cytotoxicity of human neuroblastoma. Oncogene *31*, 4859–4867.
25. Orentas, R.J., Yang, J.J., Wen, X., Wei, J.S., Mackall, C.L., and Khan, J. (2012). Identification of cell surface proteins as potential immunotherapy targets in 12 pediatric cancers. Front. Oncol. *2*, 194.
26. Almåsbak, H., Walseng, E., Kristian, A., Myhre, M.R., Suso, E.M., Munthe, L.A., Andersen, J.T., Wang, M.Y., Kvalheim, G., Gaudernack, G., and Kyte, J.A. (2015). Inclusion of an IgG1-Fc spacer abrogates efficacy of CD19 CAR T cells in a xenograft mouse model. Gene Ther. *22*, 391–403.
27. Hudecek, M., Lupo-Stanghellini, M.-T., Kosasih, P.L., Sommermeyer, D., Jensen, M.C., Rader, C., and Riddell, S.R. (2013). Receptor affinity and extracellular domain modifications affect tumor recognition by ROR1-specific chimeric antigen receptor T cells. Clin. Cancer Res. *19*, 3153–3164.
28. Long, A.H., Haso, W.M., Shern, J.F., Wanhainen, K.M., Murgai, M., Ingaramo, M., Smith, J.P., Walker, A.J., Kohler, M.E., Venkateshwara, V.R., et al. (2015). 4-1BB costimulation ameliorates T cell exhaustion induced by tonic signaling of chimeric antigen receptors. Nat. Med. *21*, 581–590.
29. Haso, W., Lee, D.W., Shah, N.N., Stetler-Stevenson, M., Yuan, C.M., Pastan, I.H., Dimitrov, D.S., Morgan, R.A., FitzGerald, D.J., Barrett, D.M., et al. (2013). Anti-CD22-chimeric antigen receptors targeting B-cell precursor acute lymphoblastic leukemia. Blood *121*, 1165–1174.
30. Long, A.H., Highfill, S.L., Cui, Y., Smith, J.P., Walker, A.J., Ramakrishna, S., El-Etriby, R., Galli, S., Tsokos, M.G., Orentas, R.J., and Mackall, C.L. (2016). Reduction of MDSCs with all-trans retinoic acid improves CAR therapy efficacy for sarcomas. Cancer Immunol. Res. *4*, 869–880.
31. Hooijberg, E., Bakker, A.Q., Ruizendaal, J.J., and Spits, H. (2000). NFAT-controlled expression of GFP permits visualization and isolation of antigen-stimulated primary human T cells. Blood *96*, 459–466.
32. Zhang, L., Kerkar, S.P., Yu, Z., Zheng, Z., Yang, S., Restifo, N.P., Rosenberg, S.A., and Morgan, R.A. (2011). Improving adoptive T cell therapy by targeting and controlling IL-12 expression to the tumor environment. Mol. Ther. *19*, 751–759.
33. Jena, B., Maiti, S., Huls, H., Singh, H., Lee, D.A., Champlin, R.E., and Cooper, L.J. (2013). Chimeric antigen receptor (CAR)-specific monoclonal antibody to detect CD19-specific T cells in clinical trials. PLoS ONE *8*, e57838.
34. Janoueix-Lerosey, I., Lequin, D., Brugières, L., Ribeiro, A., de Pontual, L., Combaret, V., Raynal, V., Puisieux, A., Schleiermacher, G., Pierron, G., et al. (2008). Somatic and germline activating mutations of the ALK kinase receptor in neuroblastoma. Nature *455*, 967–970.
35. Weijtens, M.E., Hart, E.H., and Bolhuis, R.L. (2000). Functional balance between T cell chimeric receptor density and tumor associated antigen density: CTL mediated cytolysis and lymphokine production. Gene Ther. *7*, 35–42.
36. Turatti, F., Figini, M., Balladore, E., Alberti, P., Casalini, P., Marks, J.D., Canevari, S., and Mezzanzanica, D. (2007). Redirected activity of human antitumor chimeric immune receptors is governed by antigen and receptor expression levels and affinity of interaction. J. Immunother. *30*, 684–693.
37. James, S.E., Greenberg, P.D., Jensen, M.C., Lin, Y., Wang, J., Till, B.G., Raubitschek, A.A., Forman, S.J., and Press, O.W. (2008). Antigen sensitivity of CD22-specific chimeric TCR is modulated by target epitope distance from the cell membrane. J. Immunol. *180*, 7028–7038.

38. Anurathapan, U., Chan, R.C., Hindi, H.F., Mucharla, R., Bajgain, P., Hayes, B.C., Fisher, W.E., Heslop, H.E., Rooney, C.M., Brenner, M.K., et al. (2014). Kinetics of tumor destruction by chimeric antigen receptor-modified T cells. Mol. Ther. *22*, 623–633.

39. Caruso, H.G., Hurton, L.V., Najjar, A., Rushworth, D., Ang, S., Olivares, S., Mi, T., Switzer, K., Singh, H., Huls, H., et al. (2015). Tuning sensitivity of CAR to EGFR density limits recognition of normal tissue while maintaining potent antitumor activity. Cancer Res. *75*, 3505–3518.

40. Watanabe, K., Terakura, S., Martens, A.C., van Meerten, T., Uchiyama, S., Imai, M., Sakemura, R., Goto, T., Hanajiri, R., Imahashi, N., et al. (2015). Target antigen density governs the efficacy of anti-CD20-CD28-CD3 ζ chimeric antigen receptor-modified effector CD8+ T cells. J. Immunol. *194*, 911–920.

41. Hombach, A.A., Görgens, A., Chmielewski, M., Murke, F., Kimpel, J., Giebel, B., and Abken, H. (2016). Superior therapeutic index in lymphoma therapy: CD30(+) CD34(+) hematopoietic stem cells resist a chimeric antigen receptor T-cell attack. Mol. Ther. *24*, 1423–1434.

42. Hegde, M., Mukherjee, M., Grada, Z., Pignata, A., Landi, D., Navai, S.A., Wakefield, A., Fousek, K., Bielamowicz, K., Chow, K.K., et al. (2016). Tandem CAR T cells targeting HER2 and IL13Rα2 mitigate tumor antigen escape. J. Clin. Invest. *126*, 3036–3052.

43. Itoh, Y., and Germain, R.N. (1997). Single cell analysis reveals regulated hierarchical T cell antigen receptor signaling thresholds and intraclonal heterogeneity for individual cytokine responses of CD4+ T cells. J. Exp. Med. *186*, 757–766.

44. Alvarez-Vallina, L., and Russell, S.J. (1999). Efficient discrimination between different densities of target antigen by tetracycline-regulatable T bodies. Hum. Gene Ther. *10*, 559–563.

45. James, S.E., Greenberg, P.D., Jensen, M.C., Lin, Y., Wang, J., Budde, L.E., Till, B.G., Raubitschek, A.A., Forman, S.J., and Press, O.W. (2010). Mathematical modeling of chimeric TCR triggering predicts the magnitude of target lysis and its impairment by TCR downmodulation. J. Immunol. *184*, 4284–4294.

46. Huang, J., Brameshuber, M., Zeng, X., Xie, J., Li, Q.J., Chien, Y.H., Valitutti, S., and Davis, M.M. (2013). A single peptide-major histocompatibility complex ligand triggers digital cytokine secretion in CD4(+) T cells. Immunity *39*, 846–857.

47. Srivastava, S., and Riddell, S.R. (2015). Engineering CAR-T cells: Design concepts. Trends Immunol. *36*, 494–502.

48. Ciardiello, C., Roca, M.S., Noto, A., Bruzzese, F., Moccia, T., Vitagliano, C., Di Gennaro, E., Ciliberto, G., Roscilli, G., Aurisicchio, L., et al. (2016). Synergistic antitumor activity of histone deacetylase inhibitors and anti-ErbB3 antibody in NSCLC primary cultures via modulation of ErbB receptors expression. Oncotarget *7*, 19559–19574.

49. Shimizu, R., Kikuchi, J., Wada, T., Ozawa, K., Kano, Y., and Furukawa, Y. (2010). HDAC inhibitors augment cytotoxic activity of rituximab by upregulating CD20 expression on lymphoma cells. Leukemia *24*, 1760–1768.

50. Liu, X., Jiang, S., Fang, C., Yang, S., Olalere, D., Pequignot, E.C., Cogdill, A.P., Li, N., Ramones, M., Granda, B., et al. (2015). Affinity-tuned ErbB2 or EGFR chimeric antigen receptor T cells exhibit an increased therapeutic index against tumors in mice. Cancer Res. *75*, 3596–3607.

51. Davenport, A.J., Jenkins, M.R., Cross, R.S., Yong, C.S., Prince, H.M., Ritchie, D.S., Trapani, J.A., Kershaw, M.H., Darcy, P.K., and Neeson, P.J. (2015). CAR-T Cells Inflict Sequential Killing of Multiple Tumor Target Cells. Cancer Immunol. Res. *3*, 483–494.

52. Song, D.-G., Ye, Q., Poussin, M., Liu, L., Figini, M., and Powell, D.J., Jr. (2015). A fully human chimeric antigen receptor with potent activity against cancer cells but reduced risk for off-tumor toxicity. Oncotarget *6*, 21533–21546.

53. Escors, D., Bricogne, C., Arce, F., Kochan, G., and Karwacz, K. (2011). On the Mechanism of T cell receptor down-modulation and its physiological significance. J. Biosci. Med. *1*, 2011.5.

54. Finetti, F., Onnis, A., and Baldari, C.T. (2015). Regulation of vesicular traffic at the T cell immune synapse: lessons from the primary cilium. Traffic *16*, 241–249.

55. Rachmilewitz, J., and Lanzavecchia, A. (2002). A temporal and spatial summation model for T-cell activation: signal integration and antigen decoding. Trends Immunol. *23*, 592–595.

56. Faroudi, M., Utzny, C., Salio, M., Cerundolo, V., Guiraud, M., Müller, S., and Valitutti, S. (2003). Lytic versus stimulatory synapse in cytotoxic T lymphocyte/target cell interaction: manifestation of a dual activation threshold. Proc. Natl. Acad. Sci. USA *100*, 14145–14150.

57. Huppa, J.B., and Davis, M.M. (2003). T-cell-antigen recognition and the immunological synapse. Nat. Rev. Immunol. *3*, 973–983.

58. Au-Yeung, B.B., Zikherman, J., Mueller, J.L., Ashouri, J.F., Matloubian, M., Cheng, D.A., Chen, Y., Shokat, K.M., and Weiss, A. (2014). A sharp T-cell antigen receptor signaling threshold for T-cell proliferation. Proc. Natl. Acad. Sci. USA *111*, E3679–E3688.

59. Hoffmann, D., Schott, J.W., Geis, F.K., Lange, L., Müller, F.J., Lenz, D., Zychlinski, D., Steinemann, D., Morgan, M., Moritz, T., and Schambach, A. (2017). Detailed comparison of retroviral vectors and promoter configurations for stable and high transgene expression in human induced pluripotent stem cells. Gene Ther. *24*, 298–307.

60. Kettleborough, C.A., Saldanha, J., Ansell, K.H., and Bendig, M.M. (1993). Optimization of primers for cloning libraries of mouse immunoglobulin genes using the polymerase chain reaction. Eur. J. Immunol. *23*, 206–211.

61. Sanjana, N.E., Shalem, O., and Zhang, F. (2014). Improved vectors and genome-wide libraries for CRISPR screening. Nat. Methods *11*, 783–784.

62. D'hautcourt, J.L. (2002). Quantitative flow cytometric analysis of membrane antigen expression. Curr. Protoc. Cytom. *Chapter 6*, Unit 6.12.

YMTHE, Volume *25*

Supplemental Information

Tumor Antigen and Receptor Densities Regulate Efficacy of a Chimeric Antigen Receptor Targeting Anaplastic Lymphoma Kinase

Alec J. Walker, Robbie G. Majzner, Ling Zhang, Kelsey Wanhainen, Adrienne H. Long, Sang M. Nguyen, Paola Lopomo, Marc Vigny, Terry J. Fry, Rimas J. Orentas, and Crystal L. Mackall

Supplementary Figures

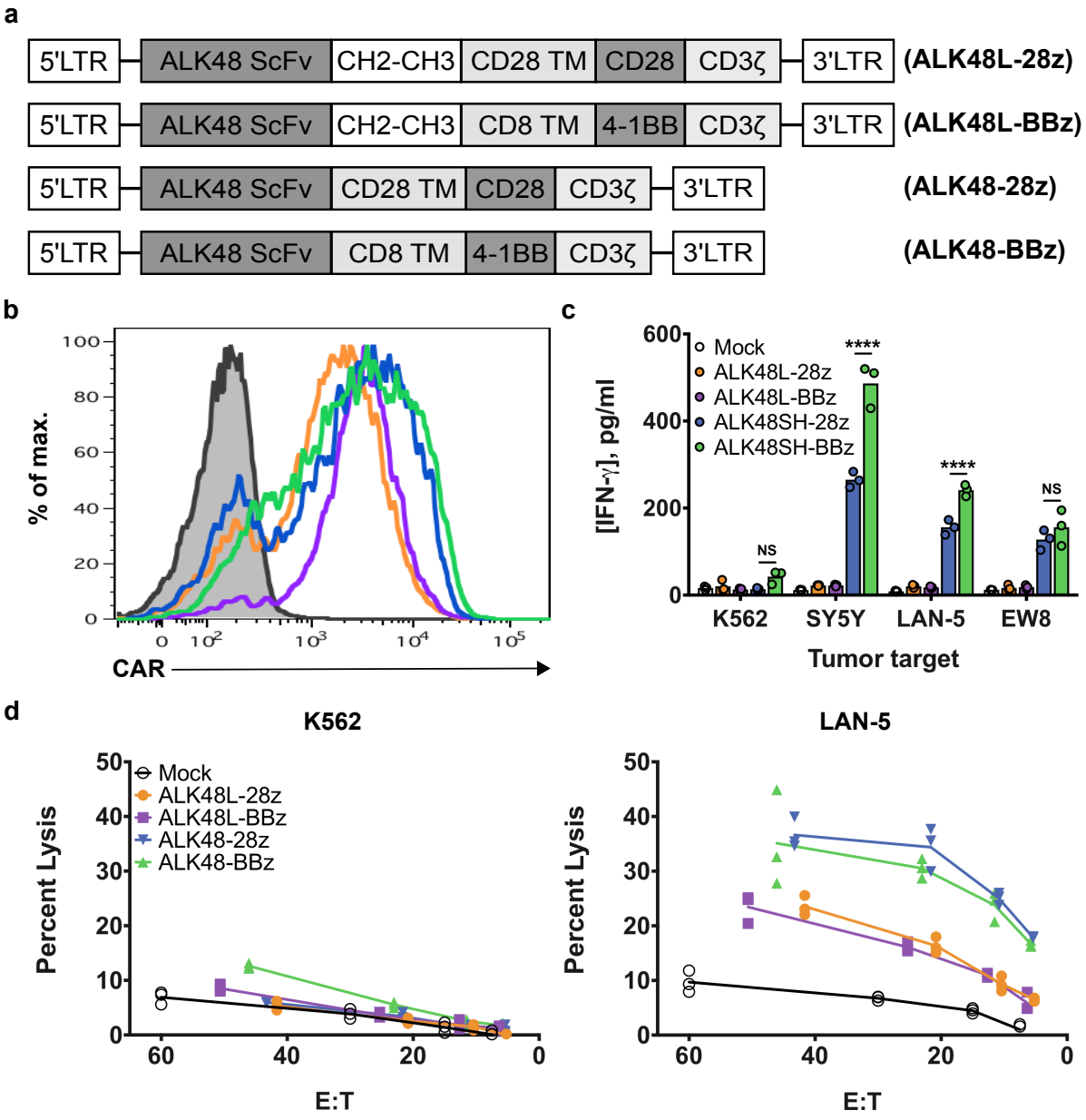

Figure S1. Characterization of ALK48 CAR T cells.

The scFv sequence of the ALK48 antibody was used to construct several CARs targeting ALK. The resulting vectors also contained either a CD28 transmembrane/co-stimulatory motif or a CD8a transmembrane/4-1BB costimulatory motif, and a CD3-zeta

signaling domain. “Long” CAR T cells were created by adding the CH2-CH3 sequence of human IgG1 between the scFv and transmembrane domains (**a**). After retroviral transduction, ALK48 CARs expressed on the surface of the human T cells (**b**). Production of IFN-gamma by ALK48 CAR T cells was evaluated after 24-hour co-incubation with ALK^+ tumor cell lines. Differences in cytokine production between CARs was determined by a two-way ANOVA followed by a Tukey’s multiple comparisons test (**c**). Cytolytic activity of ALK48 CAR T cells was assessed in a standard 6-hour ^{51}Cr release assay against ALK^- (K562) and ALK^+ (LAN-5) tumor lines (**d**). Cytokine release experiments were repeated with three different PBMC donors and cytolytic activity experiments were repeated with two different PBMC donors.

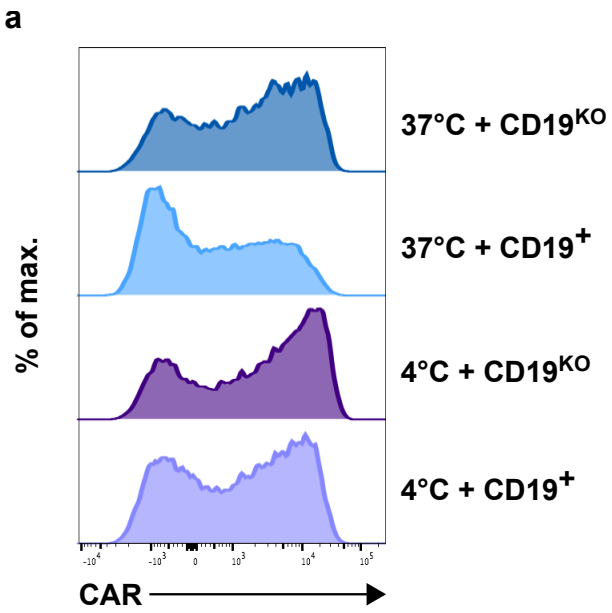

Figure S2. CARs do not down-modulate at 4°C.

CD19.4-1BB.ζ-BFP CAR T cells were co-incubated with $CD19^{+}$ or $CD19^{KO}$ NALM-6-GL tumor cells at 37°C or 4°C for 1 hour. Surface CAR was quantified by flow cytometry. Data is representative of two experiments with different donors (**a**).

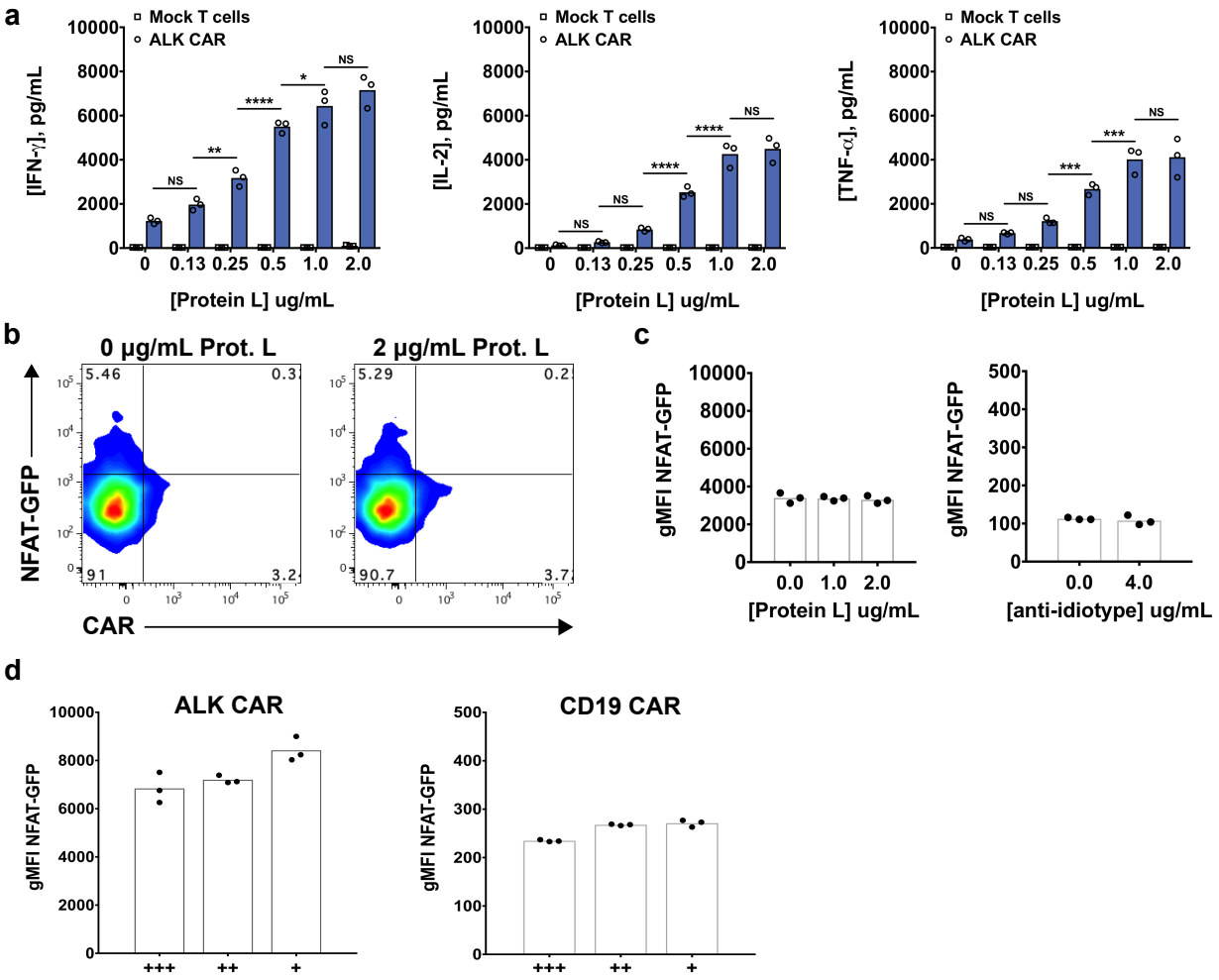

Figure S3. Evaluating CAR T cell activity with an NFAT-GFP reporter.

ALK CAR T cells were added to 96-well plates coated with a range of concentrations of biotinylated Protein L and cytokine release assayed. Differences between adjacent levels of protein L stimulation and CAR groups were determined by a two-way ANOVA followed by a Tukey's multiple comparisons test, and are representative of two experiments with different PBMC donors (**a**). Representative plots and quantification of the geometric mean fluorescence of NFAT-GFP for Mock/NFAT-GFP reporter T cells after stimulation on Protein L or anti-(CD19 scFv)-idiotype antibody coated plates are shown (**b**) and quantified (**c**). High (+++), medium

(++), or low (+) CAR expressing (ALK48.4-1BB.ζ or CD19.4-1BB.ζ-BFP)/NFAT-GFP reporter T cells were stimulated for 24 hours with anti-CD3/CD28 beads and evaluated by flow cytometry for NFAT-GFP expression (**d**). NFAT-GFP reporter data is representative of the three experiments each with the ALK CAR and CD19 CAR as described in Figure 5.